

Machine Learning Solar Wind Driving Magnetospheric Convection in Tail Lobes

Xin Cao^{1*}, Jasper S. Halekas¹, Stein Haaland², Suranga Ruhunusiri¹,
Karl-Heinz Glassmeier³

¹Department of Physics and Astronomy, University of Iowa, IA, USA.

²Birkeland Centre for Space Science, University of Bergen, Bergen, Norway.

³Institut für Geophysik und Extraterrestrische Physik, Technische Universität Braunschweig, Braunschweig, Germany.

Key Points:

- The ARTEMIS and Cluster missions observe plasma convection in the magneto-tail lobes in the far-downstream and near-Earth tail regions.
- Magnetospheric convection can be driven by the solar wind and the associated magnetospheric activity.
- Machine learning models can be used to study the potential external driving mechanism of the magnetospheric convection.

*now in University of Colorado Boulder

Corresponding author: Xin Cao, xin-cao@uiowa.edu

Abstract

To quantitatively study the driving mechanisms of magnetospheric convection in the magnetotail lobes on a global scale, we utilize data from the ARTEMIS spacecraft in the deep tail and the Cluster spacecraft in the near tail. Previous work demonstrated that, in the lobes near the Moon, we can estimate the convection by utilizing ARTEMIS measurements of lunar ions' velocity. In this paper, we analyze these datasets with machine learning models to determine what upstream factors drive the lobe convection in different magnetotail regions and thereby understand the mechanisms that control the dynamics of the tail lobes. Our results show that the correlations between the predicted and test convection velocities for the machine learning models (~ 0.75) are much better than those of the multiple linear regression model ($0.23-0.43$). The systematic analysis reveals that the IMF and magnetospheric activity play an important role in influencing plasma convection in the global magnetotail lobes.

1 Introduction

Characterizing the plasma convection in Earth's tail regions is important to help us understand the global magnetospheric dynamics. (S. Haaland et al., 2008, 2009) utilized Cluster data (Escoubet et al., 1997) to show that the plasma convection at 10 RE downtail has opposite lateral patterns in the southern and northern lobes. For instance, the convection shows a pattern such that the north-south convection moves towards the current sheet in the magnetotail. (Ohma et al., 2019) revealed that the asymmetry of the convection flow could also be affected by magnetic reconnection in the tail, which relates to magnetospheric activity. (Cao, Halekas, Chu, et al., 2020b) used the two Acceleration, Reconnection, Turbulence, and Electrodynamics of Moon's Interaction with the Sun (ARTEMIS) lunar ion data (Angelopoulos, 2011) to show that the dawn-dusk component of plasma convection velocity near the Moon's orbit (60 RE) has a high correlation with the corresponding component of the upstream Interplanetary Magnetic Field (IMF). The magnetosphere of the Earth responds to the solar wind flow and IMF, through the Dungey Cycle driven by dayside magnetic reconnection (J. W. Dungey, 1961). Based on previous studies, the magnetospheric plasma in both lobes tends to move towards the central plasma sheet. (Kisslinger et al., 2011) showed that variations in solar wind conditions can also control the magnetospheric convection. The magnitude of the convection velocity is influenced by the upstream solar wind conditions, e.g. solar wind dynamic pressure, the IMF and its clock angle, and the magnetospheric activity, as measured using the Dst (disturbance storm time) index.

The Moon has a tenuous exosphere, which is mainly composed of neutrals sourced from the surface of the Moon via various processes, e.g. solar wind sputtering, and thermal and chemical release (Stern, 1999; Sarantos et al., 2012; Cook et al., 2013; Vorburger et al., 2014), and micrometeorite impact (Hartle & Killen, 2006; Halekas et al., 2011; Horányi et al., 2015). Some of the neutral particles can be eventually transformed to same-mass heavy ions through photoionization, charge exchange, and electron impact ionization (McGrath et al., 1986; Sarantos et al., 2012; Huebner & Mukherjee, 2015; Zhou et al., 2013). The motion of lunar ions in the magnetotail lobes reflects their interaction with the exosphere, the lunar surface, and the ambient environment of the tail lobes.

Compared to other regions such as the solar wind or the magnetosheath where the ambient plasma density is much higher than that of the lunar ions (Halekas et al., 2011; Chu, Halekas, et al., 2021), the lunar ion density in the terrestrial magnetotail lobes is comparable to or even larger than that of the ambient lobe plasma, and the background flow is commonly sub-Alfvénic (Halekas et al., 2018; Liuzzo et al., 2021). Therefore, the magnetospheric tail lobes are a unique environment in which to study the dynamics of the lunar ions. In this scenario, (Cao et al., 2019; Cao, Halekas, Poppe, et al., 2020) analyzed ARTEMIS measurements to find that lunar ions are predominantly accelerated

by magnetic tension and pressure forces. As a consequence of this process, the lunar ions are eventually coupled to the ambient plasma convection by the mass loading effect. Accordingly, the plasma convection in the deep magnetotail lobes can be estimated by measurement of lunar ion motion. This technique allows ARTEMIS to estimate the convection velocity by utilizing the heavy lunar ions (which have higher energy per charge for a given convection speed), despite the fact that it cannot typically directly detect the convection of ambient low-mass ions, given the large positive spacecraft potential in the tenuous lobe environment (Cao, Halekas, Chu, et al., 2020b, 2020a).

In contrast, the convection velocity in the near-Earth tail regions can be directly measured by the Electron Drift Instrument (EDI) on the Cluster spacecraft. The EDI emits electron beams, and detect their return to the spacecraft after one or more gyrations. By continuously tracking the emitted beam, the electron gyro center drift and thus the convection can be monitored (Paschmann et al., 1997). The EDI measurement of convection velocity is not affected by the low density of ambient plasma (S. Haaland et al., 2008), and the measurement technique has been extensively validated in the magnetotail lobes (Noda et al., 2003; S. E. Haaland et al., 2007; S. Haaland et al., 2008).

Over the past few years, machine learning techniques have been widely used in space physics and planetary science (Camporeale et al., 2018). For instance, (Kerner et al., 2019) utilized a machine learning algorithm to detect novel geologic features in multispectral images of the Martian surface. (Wagstaff et al., 2019) used machine learning methods to study thermal anomalies, compositional anomalies, and plumes of icy matter from Europa's subsurface ocean. (Nguyen et al., 2019) utilized machine learning techniques to automatically detect the terrestrial bow shock and magnetopause from in-situ data, and (Lazzús et al., 2017) used machine learning algorithms to forecast the Dst index of the Earth. (Kronberg et al., 2020) utilized machine learning techniques to study solar wind control of energetic particles and X-ray.

In this paper, we used lunar ion data from the ARTEMIS spacecraft to infer lobe plasma convection velocity near the Moon in the deep magnetotail lobes (~ 60 RE), EDI measurements from Cluster to determine the convection velocity in the near-Earth magnetotail between $10 - 15$ RE, and solar wind and Dst index data from NASA's OMNI data set. We analyzed the relationship between magnetotail convection and upstream solar wind conditions and magnetospheric activity index. Based on the outputs of two ensemble learning methods: Random Forest and Gradient Boosting Decision Tree (GBDT), the results confirm that the lobe plasma convection in the tail regions is controlled by upstream solar wind and magnetospheric activity.

2 Magnetotail Observations and Model Methods

The two spacecraft of the ARTEMIS mission, P1 and P2, have been orbiting the Moon since mid-2011. We utilized measurements from two of the on-board instruments: Electrostatic Analyzer (ESA) (McFadden et al., 2008) and Flux Gate Magnetometer (FGM) (Auster et al., 2008). The ESA measures the ion distribution for energies between a few eV and 25 keV and the electron distribution for energies between a few eV and up to 30 keV (McFadden et al., 2008). The FGM measures the vector magnetic field at a cadence of 4 sec minimum. The four Cluster spacecraft fly in formation in a high inclination 4×20 RE polar orbit, with apogee in the magnetotail between August - November. From Cluster, we use EDI measurements of the convection in the tail lobes (Paschmann et al., 1997). Since the measurement regions of the two missions extend from near Earth to the Moon's orbit in the magnetotail, the coordinate system utilized in this study is Geocentric Solar Magnetospheric (GSM), in which the $+X_{\text{GSM}}$ axis is defined to be oriented towards the Sun from the center of the Earth, the $+Z_{\text{GSM}}$ axis towards the direction such that XZ plane contains the geomagnetic dipole axis, and the $+Y_{\text{GSM}}$ axis completes the right-handed system. The data utilized in this study contains over 240,000

Cluster data points in the near-Earth tail regions and over a few thousand ARTEMIS data points in the deep tail lobe regions near the Moon's orbit. The near-Earth measurement by the Cluster spacecraft was limited to be within $-8 \text{ RE} \leq \text{YGSM} \leq +8 \text{ RE}$ and $+8 \text{ RE} \leq \text{ZGSM} \leq +16 \text{ RE}$ for the northern lobe and be within $-8 \text{ RE} \leq \text{YGSM} \leq +8 \text{ RE}$ and $-16 \text{ RE} \leq \text{ZGSM} \leq -8 \text{ RE}$ for the southern lobe (S. Haaland et al., 2008). The measurements made in the deep tail lobes typically reveal a dominant positive or negative B_x component, which indicates the northern or southern lobes, respectively. As discussed in (Cao, Halekas, Chu, et al., 2020b), since the mass loading effect couples the lunar ions to the ambient plasma convection, the motion of lunar ions serves as an approximate tracer of the convection patterns in the tail lobes. More details about this method can be found in (Cao, Halekas, Poppe, et al., 2020; Cao, Halekas, Chu, et al., 2020b, 2020a; Cao et al., 2021).

The machine learning techniques we utilized in this study include random forest and GBDT, which are ensemble learning models (Friedman et al., 2001). The basic principle of this category of model is to integrate a group of weak learners into a strong learner in order to obtain a better performance, where the weak learner represents a single decision tree in the models. In contrast to a weak learner that performs at least better than random guessing, a strong learner is a model doing the prediction work as well as possible compared to the test dataset. Both random forest and GBDT utilize a data structure called decision tree as the substructure of their models. The random forest and GBDT models usually construct a number of decision trees. Each tree in the random forest model receives a sub-dataset as the training dataset, which is sampled randomly with the replacement from the whole training dataset. This resampling method is termed the Bootstrap method in statistics (Friedman et al., 2001). The key difference between the two models is that the GBDT model focuses more on the trees with larger errors during each iteration of the training process. Both the random forest and GBDT models have good ability to reduce the overfitting problem in machine learning and have been widely used in prediction and/or regression in scientific problems. The inputs of the models in this study include the solar wind IMF vector, the solar wind dynamic pressure, the local measured B_x , the Dst index, and the spacecraft locations in the magnetosphere. The Dst index describes the magnetospheric activity which can be used as an upstream monitor indirectly. The outputs of the models include the lateral components of convectional velocity: V_y and V_z . The combined training data are randomly extracted from 80% of the dataset of each mission, and other 20% of the dataset are used as the test dataset. During the training process, we also used 10-fold cross-validation (Friedman et al., 2001) to help further reduce the potential overfitting, and the optimal hyper-parameters in the models are obtained by using the grid search method. Because of the parallel computing ability, the random forest model was trained by using 8 threads simultaneously.

3 Results of Random Forest and GBDT models

The lateral component of magnetospheric convection in the lobes at different down-tail distances has been shown to correlate with the upstream solar wind IMF direction (S. Haaland et al., 2008, 2009; Cao, Halekas, Chu, et al., 2020b). The observed magnetospheric asymmetries such as dusk-dawn shift of the polar cap boundary and auroral zone flow speed asymmetry can affect the open field lines in the lobes, which may be controlled by the upstream dawn-dusk IMF (Cowley, 1981). (Tenfjord et al., 2015, 2018) utilized an MHD model to conclude that the driving mechanism might be due to the upstream lateral magnetic flux transferring to the nightside of the Earth's magnetosphere, which then affects the plasma convection in the magnetotail lobes. Convection in the Z direction is strongly influenced by dayside solar wind-magnetosphere coupling (J. Dungey, 1963). This dayside coupling is also reflected in magnetospheric disturbance indices like e.g., the Dst index, so a correlation between lobe convection and the Dst index is often

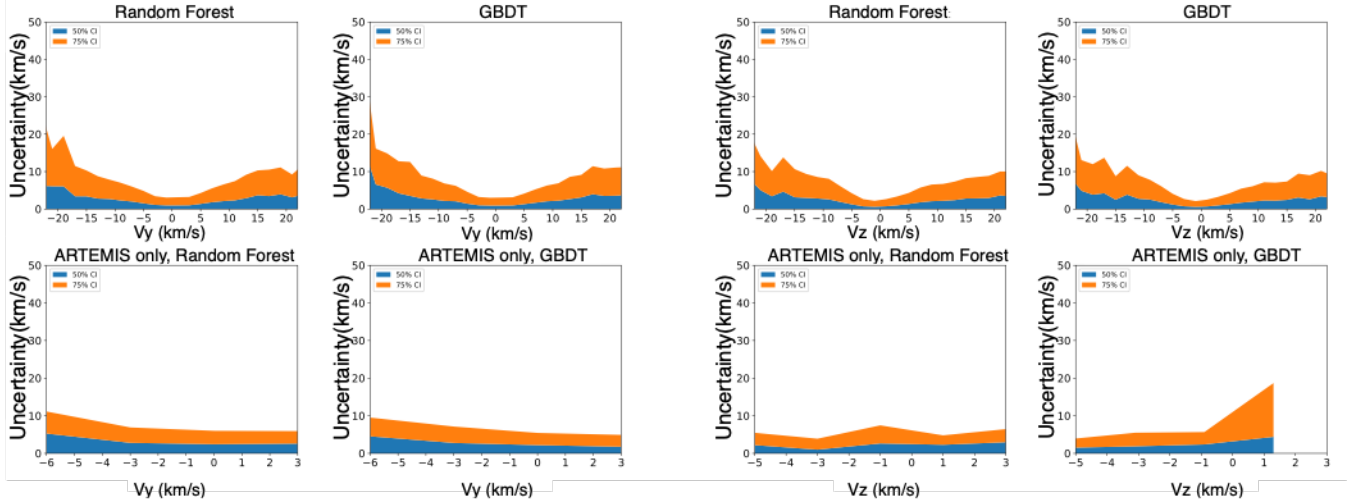


Figure 1. The 50% and 75% confidence intervals of the uncertainties (see the text) for the random forest and GBDT models respectively for V_y and V_z components of magnetospheric convection and for the near-Earth and deep magnetotail lobes. The left four panels (a) show the V_y 's and the right four panels (b) show the V_z 's.

observed (S. Haaland et al., 2009), and a larger Dst implies lower activity and thus lower convection in the tail region.

Figure 1 illustrates the uncertainties of V_y and V_z convection values predicted by the random forest and GBDT models, trained using the data set we described in the second section. The left four panels (1a) show the predicted V_y values of the random forest and GBDT models respectively for the combined data set from the two missions, and for the ARTEMIS results alone. The blue and orange colors represent the 50% and 75% confidence intervals (CI), with the uncertainties having corresponding probabilities less than the upper boundary of the shaded regions (Ruhunusiri et al., 2018). In general, the uncertainty of positive V_y is smaller than that of negative V_y . The uncertainty of V_y within 50% CI is relatively small. However, the uncertainty of V_y within 75% CI reveals somewhat larger asymmetry between positive and negative values, particularly when the velocity magnitude is larger than 15 km/s. This is probably because the proportion of the velocities with a large magnitude is much smaller than that of the velocities with a smaller magnitude, which represent the majority of the convection velocity values in the magnetotail lobes (S. Haaland et al., 2008). The relatively small proportion of larger velocity values in the data set could result in a larger bias, increasing the uncertainty of the corresponding range.

The predictions of V_y by the random forest model are better than those from the GBDT model. For the prediction of the models for the combined data set, the overall relative deviation of 50% CI's uncertainty is around 0.25, and that of 75% CI's uncertainty for the only ARTEMIS data could be up to 0.7-1.0. We will show that the predictions of these two models are much better than that of a traditional multiple linear regression model in the next section. The right four panels (1b) correspondingly show predicted V_z values for the random forest and GBDT models. As the figure shows, compared to the V_y prediction, the overall prediction of V_z by the GBDT model for the combined data set are slightly better than that of the random forest model. However, the GBDT model's prediction for the ARTEMIS measurement appears a larger uncertainty for the positive V_z . Besides, the predictions of V_y and V_z from both models for the com-

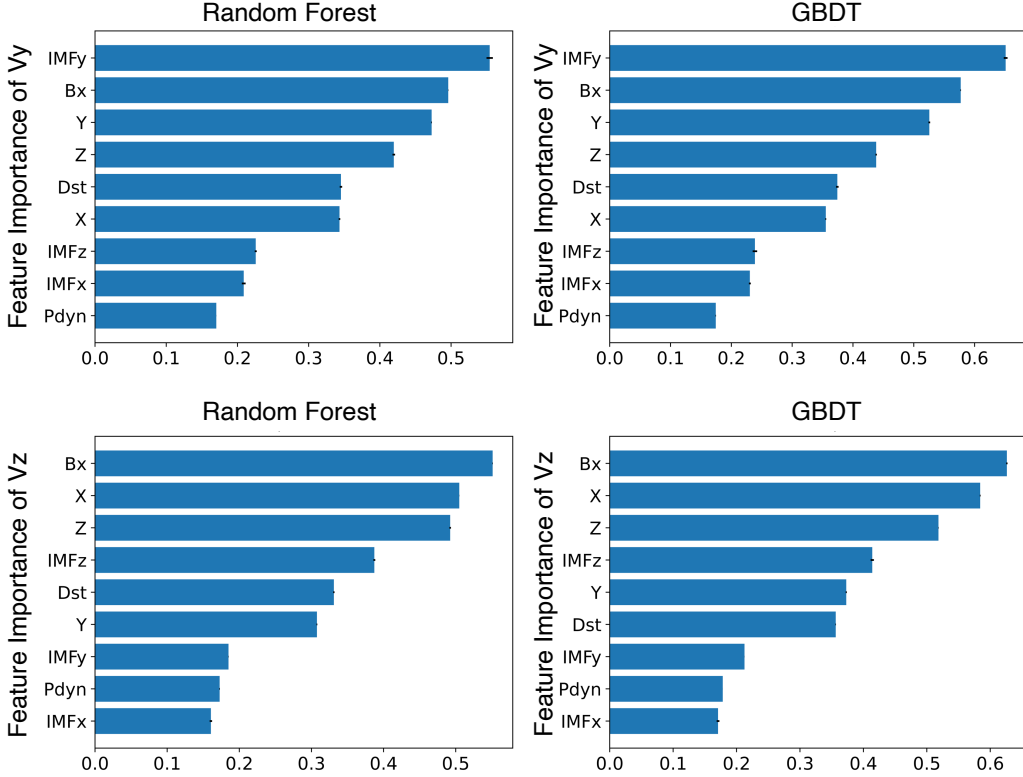


Figure 2. The feature importance of the velocity prediction for the random forest and GBDT models. The upper panels are for the V_y component of magnetotail convection and the lower panels are for V_z , respectively for the random forest and GBDT models. The error bar in black represents the standard deviation of each parameter's feature importance. The measurement locations of the spacecraft are represented by the three dimensional coordinates X, Y and Z. The IMF x , IMF y and IMF z mean the different components of the interplanetary magnetic field. The Dst index and Bx represent the magnetospheric activity index and the X component of local magnetic field in the tail lobes. The Pdyn represents the dynamic pressure of the upstream solar wind.

bined data set are better than those for the ARTEMIS data alone, likely due to a higher uncertainty in the measurement of magnetotail convection using the ARTEMIS lunar ion data.

In order to identify which input parameters are more influential in controlling the plasma convection in the magnetotail, we show the feature importance of each input parameter for the convection velocity prediction, as depicted in Figure 2. In this study, the feature importance is defined to be the score decrease of the model when randomly shuffling the values of each single feature, which indicates how much the model is dependent on that feature. We calculated 10 random shuffles for each parameter and calculated their average, in order to reduce the potential bias resulting from a single random shuffle. The results of random forest and GBDT models both reveal that the upstream IMF By has the highest feature importance for the V_y component, which indicates that it plays the biggest role of the chosen input parameters in driving the lobe convection in the magnetotail, consistent with the previous observations (Ohma et al., 2019) and (Case et al., 2018, 2020). Next, the feature importances of the local magnetic field and the Dst in-

Correlation Matrix

	X	Y	Z	IMFx	IMFy	IMFz	Bx	Pdyn	Dst	Vy	Vz
X	1.000	0.029	-0.057	-0.058	0.037	-0.015	-0.087	0.106	-0.003	0.029	0.301
Y	0.029	1.000	-0.385	-0.118	0.146	-0.077	0.071	-0.066	-0.070	0.016	-0.068
Z	-0.057	-0.385	1.000	0.080	0.002	0.076	-0.551	0.074	-0.052	0.078	-0.171
IMFx	-0.058	-0.118	0.080	1.000	-0.455	0.070	0.000	-0.114	0.011	-0.303	-0.003
IMFy	0.037	0.146	0.002	-0.455	1.000	0.014	-0.026	0.043	-0.045	0.490	-0.001
IMFz	-0.015	-0.077	0.076	0.070	0.014	1.000	-0.069	-0.005	0.202	-0.066	0.181
Bx	-0.087	0.071	-0.551	0.000	-0.026	-0.069	1.000	-0.073	0.010	-0.060	-0.172
Pdyn	0.106	-0.066	0.074	-0.114	0.043	-0.005	-0.073	1.000	0.014	0.021	0.007
Dst	-0.003	-0.070	-0.052	0.011	-0.045	0.202	0.010	0.014	1.000	-0.095	0.178
Vy	0.029	0.016	0.078	-0.303	0.490	-0.066	-0.060	0.021	-0.095	1.000	-0.075
Vz	0.301	-0.068	-0.171	-0.003	-0.001	0.181	-0.172	0.007	0.178	-0.075	1.000

Table 1. The correlation matrix between the upstream conditions and the lateral components of the convection velocity in the northern lobes throughout different tail lobe regions. The colored cells represent the correlation coefficients between each of upstream conditions and the Vy and Vz of the magnetospheric convection. Red colors indicate larger correlations and blue colors indicate larger anticorrelations.

dex are also relatively significant, which is probably linked to the fact that physical processes in the near-Earth magnetosphere, as indicated by the geomagnetic activity, have a pronounced effect on physical processes in the downstream region, due to the global disturbance of the magnetic flux transport through the magnetospheric Dungey Cycle. In contrast, the geometric locations and local magnetic field in the magnetotail lobes hold the highest feature importance for the Vz component of the convection. The Vz dynamics may be more strongly affected by the different magnetic field structure between the near-Earth and far-tail regions. The local measured Bx also plays an important role in controlling the Vz component, since its sign differs between the two lobes, with the northward-southward convection generally towards the central current sheet (S. Haaland et al., 2008; Cao, Halekas, Chu, et al., 2020b). The feature importance of the Dst index and IMFz could also be comparably important since the geomagnetic activity and the IMFz can influence the convection velocity Vz's pattern (S. Haaland et al., 2008, 2009; Ohma et al., 2019).

4 Correlation Analysis

As described in the previous sections, the magnetospheric convection in the tail lobes is largely driven by the upstream solar wind conditions and magnetospheric activity. In this section, we split the two lobes and statistically investigate the correlation between solar wind conditions and magnetospheric activity, and the plasma convection of the lobes at different down-tail distances. The correlation calculation is made by restricting the data between the 10% and 90% percentiles, in order to reduce biases from outliers.

Table 1 shows the correlation coefficients between each of the upstream parameters, the geometric locations of the measurement made in the magnetosphere, and the lateral velocity components of the magnetospheric convection in the northern lobe measured by Cluster and ARTEMIS. The correlation between the convection Vy and the IMF By has the largest value (-0.5) in the northern lobe. Corresponding, they have the largest

anti-correlation in the southern lobe. This is consistent with previous observations that showed that the dawn-dusk convection in the tail lobes is strongly controlled by the IMF By (S. Haaland et al., 2008; Case et al., 2018, 2020; Ohma et al., 2019; Cao, Halekas, Chu, et al., 2020b). The correlations between northern and southern lobes (not shown here) are similar but not exactly symmetric, which is probably due to two reasons: (1) the magnetic tilt of the Earth results in the structural asymmetry of the two lobes relative to the incident solar wind; (2) the measurement locations in the magnetosphere are not equally distributed among different lobes. The IMF By that affects the geometry of the upstream interaction with the solar wind can influence the asymmetry of the convection in the magnetosphere (Tenfjord et al., 2015).

Compared to the Vy component, the convectional Vz has a relatively significant correlation coefficient with the geometric location, which is consistent with our observation of the models. As discussed in previous section, this might be due to the influence of different magnetic field structures among different tail regions. The IMF Bz and the Dst index have comparable correlations with Vz in the two lobes, which is probably linked to the upstream reconnection-related interaction driving the magnetospheric convection, e.g. Dungey Cycle. In addition, the lateral convection of the lobes is not significantly correlated with the upstream solar wind dynamic pressure, which is consistent with previous studies (S. Haaland et al., 2008, 2009). In the global scale, the north-south component of plasma convection in the lobes (Vz) has different driving characteristics from that of Vy. For instance, the response of Vy and Vz to the Dst index appears different between the two tail lobes. The correlation of the geometric locations of the magnetosphere with Vz has also a relatively higher value compared to that with Vy, which might be because the northward-southward convection is affected by the variation of magnetic field structure from the near-Earth to the deep tail regions.

Finally, we calculated the correction between the predicted and test velocities for the two machine learning models and the multiple linear regression model. The corresponding correlation for predicted and test Vy components of random forest is 0.76, and that of GBDT is 0.75, compared to a much smaller value of 0.23 from multiple linear regression. The corresponding correlation for predicted and test Vz components of random forest is 0.78, and that of GBDT is 0.77, compared to a value of 0.43 from multiple linear regression. The comparison of the correlation coefficients between these different models confirms that the machine learning models significantly outperform the multiple linear regression.

5 Summary

In conclusion, we investigated the potential driving mechanism of the plasma convection in the magnetospheric lobes with respect to upstream solar wind conditions and geomagnetic activity, by utilizing two types of machine learning models: random forest and GBDT. We used data from the ARTEMIS and Cluster missions, and from the OMNI dataset. This study indicated that the machine learning technique could be a useful tool to predict the response of the magnetospheric convection in the tail lobes to the upstream conditions, and revealed the feature importance of each potential driving parameter, with results that appear consistent with previous studies of the convection of the tail lobes (S. Haaland et al., 2008, 2009; Ohma et al., 2019; Cao, Halekas, Chu, et al., 2020b). The ARTEMIS-Cluster-OMNI data-driven models demonstrate that the convection throughout the near-Earth and far-tail regions is largely controlled by the upstream solar wind parameters and as reflected also in magnetospheric activity indices. The IMF By values have significant correlations with the corresponding component of the convection in the tail lobes, as predicted. The geometric locations in the magnetosphere affect the Vz component more significantly than the Vy component. In addition, the Vz value in the tail lobes has a comparable response to the IMF Bz and the Dst index, which may indicate that the upstream solar wind driving mechanism consistently influences the ge-

omagnetic environment in the near-Earth magnetosphere and the downstream tail regions. This is probably associated to the global plasma dynamics, e.g. Dungey Cycle. How the dynamics of other magnetospheric regions (e.g. plasma sheet or current sheet) respond to the upstream solar wind should be addressed in future studies, as it may help build a more complete picture of the solar wind – terrestrial magnetosphere coupling processes. The method of using machine learning techniques to study the magnetospheric convection could potentially be applied to the global magnetospheres of the Earth (Liu et al., 2012) and other planets such as those of Mercury, Saturn, Jupiter, Uranus and Neptune (Cao & Paty, 2013, 2014, 2015, 2016, 2017b, 2017a, 2018, 2021) and the non-global magnetic environment such as that of Mars (Chu, Girazian, et al., 2021).

Acknowledgments

We acknowledge support from the Solar System Exploration Research Virtual Institute, Lunar Data Analysis Program grant 80NSSC20K0311, and NASA contract NAS5-02099. Karl-Heinz Glassmeier is financially supported by the German Ministerium für Wirtschaft und Energie and the Deutsches Zentrum für Luft- und Raumfahrt under contract 50 OC 1403. All ARTEMIS data are publicly available at NASA’s CDAWeb (<https://cdaweb.sci.gsfc.nasa.gov>) and the ARTEMIS site (<http://artemis.ssl.berkeley.edu>). We acknowledge James P McFadden for Electrostatic Analyzer data. We acknowledge the OMNI data which were obtained from the GSFC/SPDF OMNIWeb interface at <https://omniweb.gsfc.nasa.gov>.

References

Angelopoulos, V. (2011, December). The ARTEMIS Mission. *Space Science Reviews*, 165(1), 3–25. Retrieved from <https://doi.org/10.1007/s11214-010-9687-2> doi: 10.1007/s11214-010-9687-2

Auster, H., Glassmeier, K., Magnes, W., Aydogar, O., Baumjohann, W., Constantinescu, D., . . . others (2008). The themis fluxgate magnetometer. *Space science reviews*, 141(1-4), 235–264.

Camporeale, E., Wing, S., & Johnson, J. (2018). *Machine learning techniques for space weather*. Elsevier.

Cao, X., Halekas, J., Poppe, A., Chu, F., & Glassmeier, K. H. (2020). The acceleration of lunar ions by magnetic forces in the terrestrial magnetotail lobes. *Journal of Geophysical Research: Space Physics*, 125, 1-12. doi: 10.1029/2020JA027829

Cao, X., Halekas, J. S., Chu, F., Kistler, M., Poppe, A. R., & Glassmeier, K. (2020b). Plasma convection in the terrestrial magnetotail lobes measured near the moon’s orbit. *Geophysical Research Letters*, 47, 1-7. doi: 10.1029/2020gl090217

Cao, X., Halekas, J. S., Chu, F., Kistler, M., Poppe, A. R., & Glassmeier, K.-H. (2020a). The influence of the upstream conditions on the plasma convection in the distant tail lobes. In *Agu fall meeting abstracts* (Vol. 2020, pp. SM055–0001).

Cao, X., Halekas, J. S., Haaland, S., Ruhunusiri, S., Poppe, A. R., & Glassmeier, K.-H. (2021). Using machine learning to characterize solar wind driving of convection in the terrestrial magnetotail lobes. In *Agu fall meeting 2021*.

Cao, X., Halekas, J. S., McFadden, J. P., & Glassmeier, K.-H. (2019). The interaction of lunar ions with the ambient environment in the terrestrial magnetospheric tail lobe. In *Agu fall meeting abstracts* (Vol. 2019, pp. SM33F–3283).

Cao, X., & Paty, C. (2017b). Diurnal and seasonal variability of uranus’s magnetosphere. *Journal of Geophysical Research: Space Physics*, 122, 6318–6331. doi:

10.1002/2017JA024063

Cao, X., & Paty, C. (2021). Asymmetric structure of uranus' magnetopause controlled by imf and planetary rotation. *Geophysical Research Letters*, 48(4), e2020GL091273.

Cao, X., & Paty, C. S. (2013). Multifluid mhd simulation of the magnetosphere of uranus. *AGUFM, 2013*, SM21A-2154. Retrieved from <https://ui.adsabs.harvard.edu/abs/2013AGUFMSM21A2154C/abstract>

Cao, X., & Paty, C. S. (2014). A seasonal study of uranus' magnetosphere. *AGUFM, 2014*, SM51E-4283. Retrieved from <https://ui.adsabs.harvard.edu/abs/2014AGUFMSM51E4283C/abstract>

Cao, X., & Paty, C. S. (2015). 3d multifluid mhd simulation for uranus and neptune: the seasonal variations of their magnetosphere. *AGUFM, 2015*, SM31C-2503. Retrieved from <https://ui.adsabs.harvard.edu/abs/2015AGUFMSM31C2503C/abstract>

Cao, X., & Paty, C. S. (2016). 3d multifluid mhd simulations at uranus and neptune: Seasonal variations of their magnetospheres. *AGUFM*, SM44B-08. Retrieved from <https://ui.adsabs.harvard.edu/abs/2016AGUFMSM44B..08C/abstract>

Cao, X., & Paty, C. S. (2017a). Diurnal and seasonal variability of uranus' magnetopause under different imf. *AGUFM, 2017*, P34C-04. Retrieved from <https://ui.adsabs.harvard.edu/abs/2017AGUFM.P34C..04C/abstract>

Cao, X., & Paty, C. S. (2018). Diurnal and seasonal variability of uranus' and neptune's magnetopause under different imf. *AGUFM, 2018*, P33E-3879. Retrieved from <https://ui.adsabs.harvard.edu/abs/2018AGUFM.P33E3879C/abstract>

Case, N. A., Grocott, A., Fear, R. C., Haaland, S., & Lane, J. H. (2020, 10). Convection in the magnetosphere-ionosphere system: A multimission survey of its response to imf by reversals. *Journal of Geophysical Research: Space Physics*, 125, e2019JA027541. Retrieved from <https://onlinelibrary.wiley.com/doi/full/10.1029/2019JA027541> doi: 10.1029/2019JA027541

Case, N. A., Grocott, A., Haaland, S., Martin, C. J., & Nagai, T. (2018, 10). Response of earth's neutral sheet to reversals in the imf by component. *Journal of Geophysical Research: Space Physics*, 123, 8206-8218. Retrieved from <https://onlinelibrary.wiley.com/doi/full/10.1029/2018JA025712> doi: 10.1029/2018JA025712

Chu, F., Girazian, Z., Duru, F., Ramstad, R., Halekas, J., Gurnett, D., ... Kopf, A. (2021). The dayside ionopause of mars: Solar wind interaction, pressure balance, and comparisons with venus. *Journal of Geophysical Research: Planets*, 126(11), e2021JE006936.

Chu, F., Halekas, J. S., Cao, X., Mcfadden, J. P., Bonnell, J. W., & Glassmeier, K.-H. (2021). Electrostatic waves and electron heating observed over lunar crustal magnetic anomalies. *Journal of Geophysical Research: Space Physics*, 126(4), e2020JA028880.

Cook, J. C., Stern, S. A., Feldman, P. D., Gladstone, G. R., Rutherford, K. D., & Tsang, C. C. (2013, 7). New upper limits on numerous atmospheric species in the native lunar atmosphere. *Icarus*, 225, 681-687. doi: 10.1016/J.ICARUS.2013.04.010

Cowley, S. W. (1981). Magnetospheric asymmetries associated with the y-component of the imf. *Planetary and Space Science*, 29, 79-96. doi: 10.1016/0032-0633(81)90141-0

Dungey, J. (1963). Interactions of solar plasma with the geomagnetic field. *Planetary and Space Science*, 10, 233-237.

Dungey, J. W. (1961, Jan). Interplanetary magnetic field and the auroral zones. *Phys. Rev. Lett.*, 6, 47-48. Retrieved from <https://link.aps.org/doi/10.1103/PhysRevLett.6.47> doi: 10.1103/PhysRevLett.6.47

Escoubet, C., Schmidt, R., & Goldstein, M. (1997, January). CLUSTER – SCIENCE AND MISSION OVERVIEW. *Space Science Reviews*, 79(1), 11–32. Retrieved from <https://doi.org/10.1023/A:1004923124586> doi: 10.1023/A:1004923124586

Friedman, J., Hastie, T., Tibshirani, R., et al. (2001). *The elements of statistical learning* (Vol. 1) (No. 10). Springer series in statistics New York.

Haaland, S., Lybekk, B., Svenes, K., Pedersen, A., Förster, M., Vaith, H., & Torbert, R. (2009). Plasma transport in the magnetotail lobes. *Annales Geophysicae*, 27, 3577–3590. doi: 10.5194/angeo-27-3577-2009

Haaland, S., Paschmann, G., Förster, M., Quinn, J., Torbert, R., Vaith, H., ... Kletzing, C. (2008). Plasma convection in the magnetotail lobes: Statistical results from cluster edi measurements. *Annales Geophysicae*, 26, 2371–2382. doi: 10.5194/angeo-26-2371-2008

Haaland, S. E., Paschmann, G., Förster, M., Quinn, J. M., Torbert, R. B., McIlwain, C. E., ... Kletzing, C. A. (2007). High-latitude plasma convection from cluster edi measurements: Method and imf-dependence. *Annales Geophysicae*, 25, 239–253. doi: 10.5194/angeo-25-239-2007

Halekas, J. S., McFadden, J. P., Plaschke, F., Bonnell, J. W., Fillingim, M. O., Farrell, W. M., ... Angelopoulos, V. (2011). First remote measurements of lunar surface charging from artemis: Evidence for nonmonotonic sheath potentials above the dayside surface. *Journal of Geophysical Research: Space Physics*, 116, n/a-n/a. doi: 10.1029/2011ja016542

Halekas, J. S., Poppe, A. R., Harada, Y., Bonnell, J. W., Ergun, R. E., & McFadden, J. P. (2018). A tenuous lunar ionosphere in the geomagnetic tail. *Geophysical Research Letters*, 45, 9450–9459. doi: 10.1029/2018GL079936

Hartle, R. E., & Killen, R. (2006). Measuring pickup ions to characterize the surfaces and exospheres of planetary bodies: Applications to the moon. *Geophysical Research Letters*, 33, 2–6. doi: 10.1029/2005GL024520

Horányi, M., Szalay, J., Kempf, S., Schmidt, J., Grün, E., Srama, R., & Sternovsky, Z. (2015). A permanent, asymmetric dust cloud around the moon. *Nature*, 522(7556), 324–326.

Huebner, W., & Mukherjee, J. (2015). Photoionization and photodissociation rates in solar and blackbody radiation fields. *Planetary and Space Science*, 106, 11–45.

Kerner, H. R., Wellington, D. F., Wagstaff, K. L., Bell, J. F., Kwan, C., & Amor, H. B. (2019). Novelty detection for multispectral images with application to planetary exploration. In *Proceedings of the aaai conference on artificial intelligence* (Vol. 33, pp. 9484–9491).

Kissinger, J., McPherron, R., Hsu, T.-S., & Angelopoulos, V. (2011). Steady magnetospheric convection and stream interfaces: Relationship over a solar cycle. *Journal of Geophysical Research: Space Physics*, 116(A5).

Kronberg, E. A., Gastaldello, F., Haaland, S., Smirnov, A., Berrendorf, M., Ghizardi, S., ... others (2020). Prediction and understanding of soft-proton contamination in xmm-newton: A machine learning approach. *The Astrophysical Journal*, 903(2), 89.

Lazzús, J., Vega, P., Rojas, P., & Salfate, I. (2017). Forecasting the dst index using a swarm-optimized neural network. *Space Weather*, 15(8), 1068–1089.

Liu, Z.-Q., Lu, J., Kabin, K., Yang, Y., Zhao, M., & Cao, X. (2012). Dipole tilt control of the magnetopause for southward imf from global magnetohydrodynamic simulations. *Journal of Geophysical Research: Space Physics*, 117(A7).

Liuzzo, L., Poppe, A. R., Halekas, J. S., Simon, S., & Cao, X. (2021). Investigating the moon's interaction with the terrestrial magnetotail lobe plasma. *Geophysical Research Letters*, 48(9), e2021GL093566.

McFadden, J. P., Carlson, C. W., Larson, D., Ludlam, M., Abiad, R., Elliott, B., ... Angelopoulos, V. (2008). The themis esa plasma instrument

and in-flight calibration. *Space Science Reviews*, *141*, 277-302. doi: 10.1007/s11214-008-9440-2

McGrath, M., Johnson, R., & Lanzerotti, L. (1986). Sputtering of sodium on the planet mercury. *Nature*, *323*(6090), 694–696.

Nguyen, G., Aunai, N., Michotte de Welle, B., Jeandet, A., & Fontaine, D. (2019). Automatic detection of the earth bow shock and magnetopause from in-situ data with machine learning. *Annales Geophysicae Discussions*, 1–22.

Noda, H., Baumjohann, W., Nakamura, R., Torkar, K., Paschmann, G., Vaith, H., ... Quinn, J. M. (2003). Tail lobe convection observed by cluster/edi. *Journal of Geophysical Research: Space Physics*, *108*, 1-7. doi: 10.1029/2002JA009669

Ohma, A., Østgaard, N., Reistad, J. P., Tenfjord, P., Laundal, K. M., Jørgensen, T. M., ... Milan, S. (2019). Observations of asymmetric lobe convection for weak and strong tail activity. *Journal of Geophysical Research: Space Physics*, *124*, 9999-10017. doi: 10.1029/2019JA026773

Paschmann, G., Melzner, F., Frenzel, R., Vaith, H., Parigger, P., Pagel, U., ... others (1997). The electron drift instrument for cluster. *Space Science Reviews*, *79*(1), 233–269.

Ruhunusiri, S., Halekas, J. S., Espley, J. R., Eparvier, F., Brain, D., Mazelle, C., ... Jakosky, B. M. (2018). An artificial neural network for inferring solar wind proxies at mars. *Geophysical Research Letters*, *45*, 10,855-10,865. doi: 10.1029/2018GL079282

Sarantos, M., Hartle, R. E., Killen, R. M., Saito, Y., Slavin, J. A., & Glocer, A. (2012). Flux estimates of ions from the lunar exosphere. *Geophysical Research Letters*, *39*, 6-11. doi: 10.1029/2012GL052001

Stern, S. A. (1999, 11). The lunar atmosphere: History, status, current problems, and context. *Reviews of Geophysics*, *37*, 453-491. Retrieved from <https://onlinelibrary.wiley.com/doi/full/10.1029/1999RG900005> doi: 10.1029/1999RG900005

Tenfjord, P., Østgaard, N., Haaland, S., Snekvik, K., Laundal, K. M., Reistad, J. P., ... Ohma, A. (2018). How the imf by induces a local by component during northward imf bz and characteristic timescales. *Journal of Geophysical Research: Space Physics*, *123*, 3333-3348. doi: 10.1002/2018JA025186

Tenfjord, P., Østgaard, N., Snekvik, K., Laundal, K. M., Reistad, J. P., Haaland, S., & Milan, S. E. (2015). How the imf b y induces a b y component in the closed magnetosphere and how it leads to asymmetric currents and convection patterns. *Journal of Geophysical Research : Space Physics*. doi: 10.1002/2015JA021579. Received

Vorburger, A., Wurz, P., Barabash, S., Wieser, M., Futaana, Y., Holmström, M., ... Asamura, K. (2014). First direct observation of sputtered lunar oxygen. *Journal of Geophysical Research: Space Physics*, *119*(2), 709–722.

Wagstaff, K. L., Doran, G., Davies, A., Anwar, S., Chakraborty, S., Cameron, M., ... Phillips, C. (2019). Enabling onboard detection of events of scientific interest for the europa clipper spacecraft. In *Proceedings of the 25th ACM sigkdd international conference on knowledge discovery & data mining* (pp. 2191–2201).

Zhou, X.-Z., Angelopoulos, V., Poppe, A. R., & Halekas, J. S. (2013). Artemis observations of lunar pickup ions: Mass constraints on ion species. *Journal of Geophysical Research: Planets*, *118*, 1766-1774. doi: 10.1002/jgre.20125